Predicting critical currents in grain-boundary limited superconductors

M. Eisterer

Atominstitut, TU Wien, Stadionallee 2, 1020 Vienna, Austria

The critical current across grain boundaries is severely suppressed in high-temperature superconductors, such as the cuprate and iron-based compounds, if the grain boundary angle exceeds a few degrees. This is known from the low critical currents in untextured conductors and measurements on bicrystalline films. Textured conductors were developed to overcome this limitation; however, a quantitative understanding between the degree of texture and the macroscopic critical current is still missing. A model for the prediction of the self-field critical current as a function of grain alignment on the basis of experimental data obtained from bicrystals is presented. It is a mean-field approach based on percolation theory. Without any fit parameter, good agreement with recent studies on cuprates and iron-based superconductors is obtained, where the critical current and the texture were analyzed quantitatively. The simplified grain boundary physics hence describes the macroscopic properties of imperfectly textured materials.

I. INTRODUCTION

Many exciting superconducting materials have been discovered in the past decades. They are very promising for applications since they can significantly extend the operational space of superconductivity in terms of both temperature and magnetic field. The most promising among them, the cuprate and iron-based superconductors, suffer from a bad connectivity between the grains of a conductor. It was shown for bicrystalline films that the critical current across grain boundaries drops exponentially with the misalignment angle between adjacent grains [1,2]. The technological solution of this problem was the development of textured conductors, the most efficient form being coated conductors, where the grains are aligned within a few degrees so that they are sometimes called "single crystals by the mile." However, the corresponding production processes are slow and expensive; hence, the market is still dominated by NbTi and Nb_3Sn, which do not suffer from this granularity problem. Alternative texturing processes, in particular thermomechanical treatments, are cheaper, but the resulting grain alignment is less perfect. Recent results on Bi-2212 [3,4] and Ba-122 [5] indeed indicate the feasibility of this approach. The relation between texture and the macroscopic critical current density is still not understood quantitatively despite many approaches, such as the brick-wall [6,7], railway switch [8], freeway [9], and parallel path [10] models, and various numerical approaches [11–15]. Most of them model the current meandering between the grains to predict the macroscopic behavior. Here, the approach is different, focusing on only the statistical distribution of the grain boundary angles and neglecting any details of the grain structure or its local variation. This enables a comparison of different materials on the basis of the experimentally observed dependence of the critical current density on the misalignment angle and a quantitative prediction of the influence of texture.

II. MEAN-FIELD PERCOLATION MODEL

The percolation model is based on the mean-field approach originally proposed for predicting the critical current density in MgB_2 [16], as well as its anisotropy upon texturing [17]. While the anisotropy of the upper critical field induces a variation of the properties of differently oriented grains and hence causes the inhomogeneity of the current flow in MgB_2, the grain boundary currents are assumed to vary and limit, per definition, the macroscopic currents in grain-boundary-limited superconductors. The critical current density J_c is obtained from a simple integral [16],

$$J_c = \int_0^{J_c^{\max}} \sigma_p dJ. \tag{1}$$

It basically sums up infinitesimal current densities weighted by the effective cross section

$$\sigma_p = \left(\frac{p(J) - p_c}{1 - p_c} \right)^t \tag{2}$$

over which they flow. The higher the local current density is, the smaller the effective cross section becomes because fewer current paths are available for higher currents. σ_p is motivated by percolation theory, with $p(J)$ being the fraction of sites (grains) or bonds (grain boundaries) having a local critical current density $J_c^{G/GB}$ exceeding J. If this fraction decreases to the percolation threshold p_c, σ_p becomes zero because no continuous current path can be formed at smaller p. (The spanning cluster decomposes into separated clusters.) p_c is about 0.2 in three-dimensional systems and depends on the coordination number, i.e., the number of neighboring grains. It is generally somewhat smaller in bond than in site percolation problems because removing one site removes all respective bonds, while a site may stay connected with the spanning
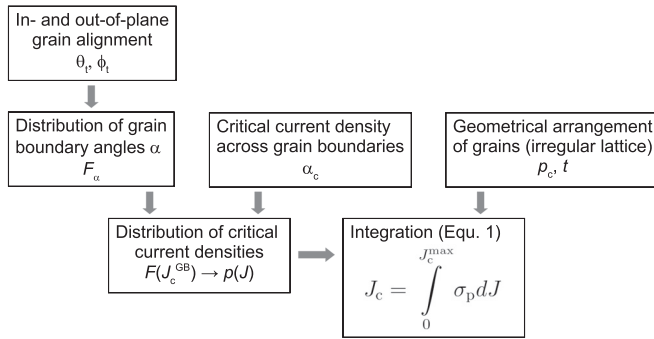
FIG. 1. Diagram of the percolation model.

cluster upon removing one of its bonds. Its actual value is hard to assess in real systems, but it can be calculated for regular lattices; for example, a value of 0.2487 results for a simple cubic lattice (coordination number of 6), and a value of 0.1802 results for a bcc lattice (coordination number of 8) [18]. For the sake of simplicity and to keep the number of free parameters small, $p_c = 0.2$ will be used in the following. The so-called transport exponent t was fixed to 1.76, as expected for three-dimensional systems in the highly nonlinear limit [19]. $p(J)$ hence contains all information on the actual material. It is just $1 - F(J)$, with the distribution function of the critical current densities $F(J_c^{GB})$. (The following refers to only grain boundary currents since they are the focus of this study.) J_c^{max} is given by the condition $p(J_c^{max}) = p_c$, where the effective cross section becomes zero because grain boundaries with higher critical current densities do not form a continuous cluster anymore and therefore cannot contribute more than J_c^{max} to the macroscopic current.

A sketch of the percolation model is shown in Fig. 1. In addition to p_c and t, $F(J_c^{GB})$ has to be known or modeled in order to get the macroscopic critical current density by means of Eq. (1). This is very complex for the general case due to the large variety of possible grain boundaries. Five parameters are needed to classify them: the grain boundary angle α, the orientation of the rotational (or common) axis (two parameters), and the grain boundary plane (two parameters).

Figure 2 illustrates a grain boundary and the respective grain boundary angle. Assuming the crystallographic axes are parallel to the edges of the grains (cuboids) and the rotational axis is parallel to the c axis, Fig. 2 would sketch a [001] tilt boundary. This is, however, not the general case because the orientation of the rotational axis and the grain boundary plane can be chosen arbitrarily. A model and experimental data for J_c as a function of all five parameters are currently
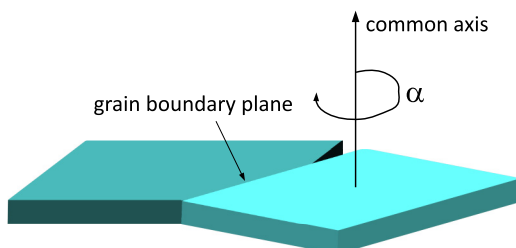
unavailable, and we restrict our considerations to the grain boundary angle α. Most available experimental data refer to [001] tilt boundaries (e.g., [1] and references therein), and an exponential decrease of J_c as a function of α was found after a plateau at low angles in the cuprates [1] as well as in the iron-based superconductors [2,20],

$$J_c^{GB} = J_0 e^{-1} \quad \text{for } \alpha \leqslant \alpha_c, \tag{3}$$

$$J_c^{GB} = J_0 e^{-\frac{\alpha}{\alpha_c}} \quad \text{for } \alpha \geqslant \alpha_c. \tag{4}$$

Although the actual type of grain boundary [21] and its morphology [22] influence this dependence, the exponential behavior is a general trend in these two classes of superconductors, and the critical currents across grain boundaries will be modeled by Eqs. (3) and (4). With this simplification, $F(J_c^{GB})$ and $p(J)$ needed for the integral in Eq. (1) can be calculated from the distribution function of the grain boundary angle F_α, which will be derived in the following.

A. Distribution of grain boundary angles

We consider first the distribution of grain boundary angles between two arbitrarily oriented grains. The orientation of one grain can be obtained from the orientation of the other grain by the rotation about the common axis (see Fig. 2). The respective rotation angle defines the grain boundary angle α. For a totally random orientation of both grains this results, for $0 \leqslant \alpha \leqslant \pi$, in (details are given in the Appendix)

$$f_\alpha(\alpha) = \frac{1 - \cos\alpha}{2\pi}, \tag{5}$$

$$F_\alpha(\alpha) = \frac{\alpha - \sin\alpha}{2\pi}, \tag{6}$$

where $f_\alpha(\alpha)$ denotes the distribution density of the distribution function $F_\alpha(\alpha)$, i.e., $f_\alpha(\alpha) = F'_\alpha(\alpha)$. The angular range is restricted to 180° since clockwise and counterclockwise rotations lead to the same boundary. However, there are further symmetries because a rotation about 180° results in the same crystal lattice. We further assume that the effect of orthorhombicity is small; hence, rotations about the crystallographic c axis have a periodicity of 90°. This leads to

$$F_\alpha(\alpha) = \frac{8}{\pi}(\alpha - \sin\alpha) \tag{7}$$

for $\alpha \leqslant \frac{\pi}{4}$,

$$F_\alpha(\alpha) = 2 - \frac{8}{\pi}(\cos\alpha + 1)\tan\frac{\pi}{8} \tag{8}$$

for $\frac{\pi}{4} \leqslant \alpha \leqslant \frac{\pi}{2}$, and approximately

$$F_\alpha(\alpha) \approx 2 - \frac{4}{\pi}\arccos(2\cos\alpha + 1) - \frac{8}{\pi}(\cos\alpha + 1)\left(\tan\frac{\pi}{8}\right.$$
$$\left. - \tan\frac{\arccos(2\cos\alpha + 1)}{2}\right) \tag{9}$$

for $\frac{\pi}{2} \leqslant \alpha \leqslant 1.7178$. (The derivation of the maximum of α can be found in the Appendix.)

The distribution function (bottom panel) and the distribution density (top panel) are shown as gray lines in Fig. 3. The circles in Fig. 3 were obtained from numerical simulations

FIG. 2. Sketch of a grain boundary.
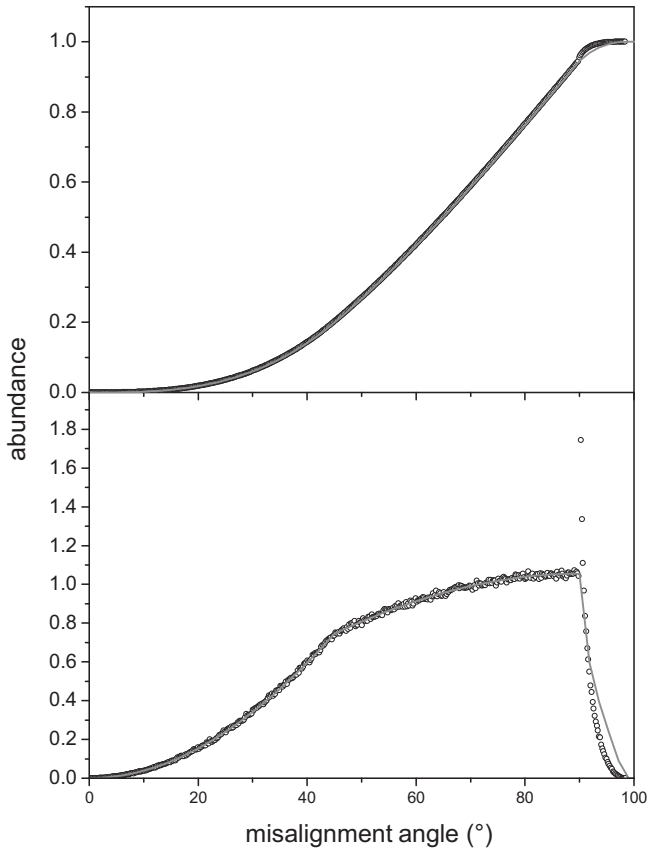
FIG. 3. Distribution function (top panel) and distribution density (bottom panel) of grain boundary angles for randomly oriented grains. The line graphs were obtained from the analytical expressions [see Eqs. (7)–(9)]; the circles represent the results from the simulation.

FIG. 4. Distribution density of the grain boundary angles for uniaxial (top panel) and biaxial (bottom panel) textures. The given angles refer to the out-of-plane texture angle θ_t. $\phi_t = \theta_t$ is assumed for biaxial texture; $\phi_t = \infty$ is assumed for uniaxial texture. The distribution densities were divided by 2 and 5 for $\phi_t = 5°$ and $1°$, respectively, to fit into the bottom panel.

assuming cubic grains on a simple cubic lattice. The orientation of the grains was chosen randomly, and the distribution density was obtained by counting the grain boundary angles in a small angular range. Details are given in the Appendix. These simulations are necessary to obtain the distribution of grain boundary angles in textured samples, as well as to ensure that the distribution is also valid for a large ensemble of grains. The analytical expressions are valid for the distribution of two grains with random orientation, but the grain boundary angles are not independent of each other in a large ensemble, which becomes evident by considering a closed path containing an arbitrary number of grains. The grain boundary angles are restricted by the condition that the grain orientation has to be the same after the entire loop. Although this restriction does not change the angular distribution in an ensemble of randomly oriented grains, it does for partially aligned grains (not shown), and the maximum in the grain boundary angle distribution density of the ensemble shifts to lower angles compared to the case of two grains.

The differences between the analytical formula and the simulation for grain boundaries above 90° are caused by something else: the derivation of the formula does not take all symmetries into account [see Eq. (A8) in the Appendix]. These symmetries reduce some of the grain boundary angles for $\frac{\pi}{2} \leqslant \alpha \leqslant 1.7178$, but they remain in this angular range and

cause the discontinuity (appearing as spikes in Figs. 3 and 4) at 90° in the distribution density. (The distribution function changes slope.)

A first important result follows from the grain boundary angle distribution between randomly oriented grains. The distribution function becomes 0.2, which is a typical percolation threshold in three-dimensional materials, only at about 45° (top panel in Fig. 3). Since nearly all experimental data for critical currents across grain boundaries were obtained for bicrystals with misorientation angles up to 45° [1], these data are not useful for predicting the behavior of untextured materials. If the fraction of grain boundaries with angles below 45° is smaller than the percolation threshold, these boundaries can, by definition, not form a continuous current path throughout the entire sample and, consequently, cannot contribute more to the global currents than the best links in the remaining matrix. Data for grain boundaries with grain boundary angles above 45° are needed for modeling untextured superconductors. We will restrict our considerations in the following to textured samples, where the grain boundaries below 45° determine the properties, so that the behavior known from experiments can be used [i.e., Eqs. (3) and (4)].

B. Preferred grain orientation

A Gaussian distribution density of the grain misalignment from the preferred orientation is assumed:

$$f(\theta) \propto e^{-\frac{\theta^2}{2\theta_t^2}} \sin\theta, \tag{10}$$

$$f(\phi) \propto e^{-\frac{\phi^2}{2\phi_t^2}}, \tag{11}$$

where the texture angles ϕ_t and θ_t quantify the in- and out-of-plane textures, respectively. Since $f(\phi)$ becomes $\frac{1}{2}$ at $\phi = \sqrt{2\ln 2}$, the full width at half maximum is larger by a factor of $2\sqrt{2\ln 2} \approx 2.35$ than these texture angles. (A Gaussian distribution of the out-of-plane orientation was indeed found in weakly textured MgB_2 [23].)

The top panel in Fig. 4 shows the evolution of the grain boundary angle distribution density with texture for the pure out-of-plane texture, as achieved, for instance, by thermomechanical treatments (see Bi-2223 below). With decreasing θ_t, a peak evolves below $90°$ and shifts to lower angles upon improving texture. A plateau develops below $45°$ which finally extends to $0°$ in the limit $\theta_t = 0$ when the peak disappears, reflecting the equal distribution of the in-plane misorientation angle ϕ.

This plateau does not occur for the biaxial texture. The distribution densities displayed in the bottom panel of Fig. 4 were calculated for $\phi_t = \theta_t$, meaning the same in- and out-of-plane alignments. There is hardly any difference from uniaxial texture at $\theta_t = 45°$, some weight is transferred to grain boundary angles below $45°$ at $\theta_t = 30°$, and the peak shifts from $45°$ to about $25°$ for $\theta_t = 15°$, becoming more symmetric for biaxial grain alignment. At lower texture angles, the distribution functions become very different because of the absence of the plateau. The distribution density has to converge to the δ function for $\theta_t = \phi_t \rightarrow 0°$.

We will restrict our considerations in the following to textured samples with texture angles below $15°$, where grain boundaries below $45°$ determine the properties so that the available experimental data can be used. Figure 5 demonstrates the influence of texture on J_c. The open and solid symbols refer to uniaxial ($\phi_t = \infty$) and biaxial ($\phi_t = \theta_t$) textures. The decay angle α_c in Eq. (4) was chosen to be 5 and 9 for cuprate and iron-based superconductors [1,2,20]. The top panel represents the suppression of J_c; the data are normalized by J_0/e [see Eq. (4)]. In the case of uniaxial texture, a plateau is found at low angles in both materials, where the in-plane misorientation dominates. It is evident that a large decay angle α_c in Eq. (4) is crucial for large currents in the case of the pure out-of-plane texture. The currents are suppressed to 9% and 1.5% for the perfect out-of-plane texture ($\theta_t = 0$) in iron-based ($\alpha_c = 9°$) and cuprate ($\alpha_c = 5°$) superconductors, respectively. The low-angle plateau is restricted to very small angles in the case of the biaxial texture, when all misorientation angles are below α_c and the grain boundaries do not limit the currents anymore. If the texture becomes weaker, α_c determines the slope of the approximately exponential decrease in J_c with θ_t for both uni- and biaxial textures.

The percolation threshold p_c was fixed to 0.2 in this study, but it varies and is hard to determine in a real system. To
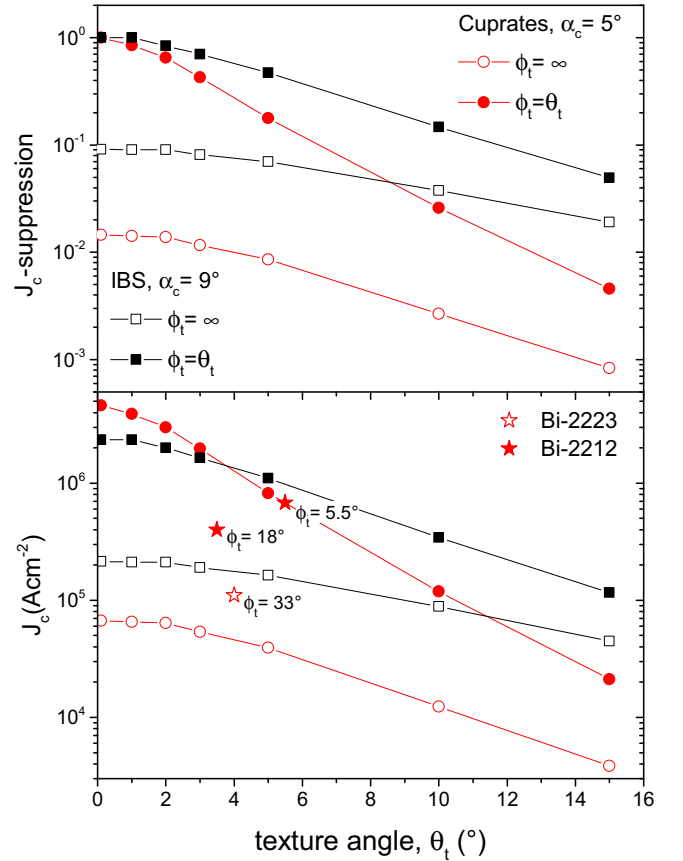
FIG. 5. Critical current densities as a function of texture quantified by θ_t. The current densities are normalized by the intragranular value (i.e., $\alpha = 0$) in the top panel. The expected values of J_0 for Bi-2212/2223 and K-doped Ba-122 were used to calculate the current densities shown in the bottom panel.

investigate the importance of this parameter, the J_c suppression in the case of perfect uniaxial (out-of-plane) alignment was recalculated for $p_c = 0.15$ and $p_c = 0.25$, which bound the realistic range of p_c. A smaller J_c reduction to 11.6% and 2.3% is found for iron-based and cuprate superconductors with $p_c = 0.15$, while an increase of p_c to 0.25 results in a smaller J_c (7.2% and 0.9% of J_0/e, respectively). A change in p_c in the realistic range causes a similar relative change in J_c. Although p_c does influence the absolute values of the critical currents, slight changes in p_c do not alter the results and conclusions of this study qualitatively.

The positive effect of the larger α_c in the iron-based superconductors is partly compensated by a smaller J_0. For instance, J_0 was reported to be $2.8 \times 10^6 \, \mathrm{A\,cm^{-2}}$ for Co-doped Ba-122 [2], and the data for $YBa_2Cu_3O_{7-\delta}$ (YBCO) summarized in Fig. 30 of the review by Hilgenkamp and Mannhart [1] indicate J_0 is about $2 \times 10^7 \, \mathrm{A\,cm^{-2}}$. Many fewer data obtained from bicrystals are available for other compounds of these superconducting families. Since the properties of $Bi_2Sr_2Ca_nCu_{n+1}O_{2n+6}$ (BiSSCO) and K-doped Ba-122 tapes and wires will be discussed later, J_0 of these compounds has to be estimated. The maximum current density that can be obtained in superconductors scales with the depairing current density J_d; it seems hence reasonable to rescale J_0 with the

respective depairing current densities, which are about 400, 240, 110, and 75 MA cm^{-2} in YBCO, BiSCCO (similar for 2212 and 2223), and K- and Co-doped Ba-122, respectively. This leads to $J_0 \approx 1.25 \times 10^7$ A cm^{-2} for BiSCCO 2212 and 2223 and $J_0 \approx 6.35 \times 10^6$ A cm^{-2} for K-doped Ba-122. These data refer to low temperatures (around 4.2 K) and self-field. The resulting current densities in granular conductors are shown in the bottom panel of Fig. 5. Iron-based superconductors are favorable compared to the cuprates for uniaxially textured conductors considering the grain alignment. The situation is more complex in biaxially textured conductors where the cuprates (BiSSCO) reach higher currents at high texture but fall below J_c of K-doped Ba-122 at around $\theta_t = 5°$. The situation is even more favorable for YBCO since its J_d and hence J_0 are higher.

III. COMPARISON WITH EXPERIMENTAL DATA

The excellent work of Kametani *et al.* [24] provides data on texture obtained from electron backscatter diffraction orientation imaging microscopy (EBSD-OIM) together with critical current densities of the same conductor. This is ideal for checking the predictions of the calculations and validating the underlying, simplified grain boundary physics. The top panel in Fig. 6 compares the experimentally obtained distribution density of the grain boundary angles in a Bi-2223 tape with the theoretical expectation. The gray line corresponds to the
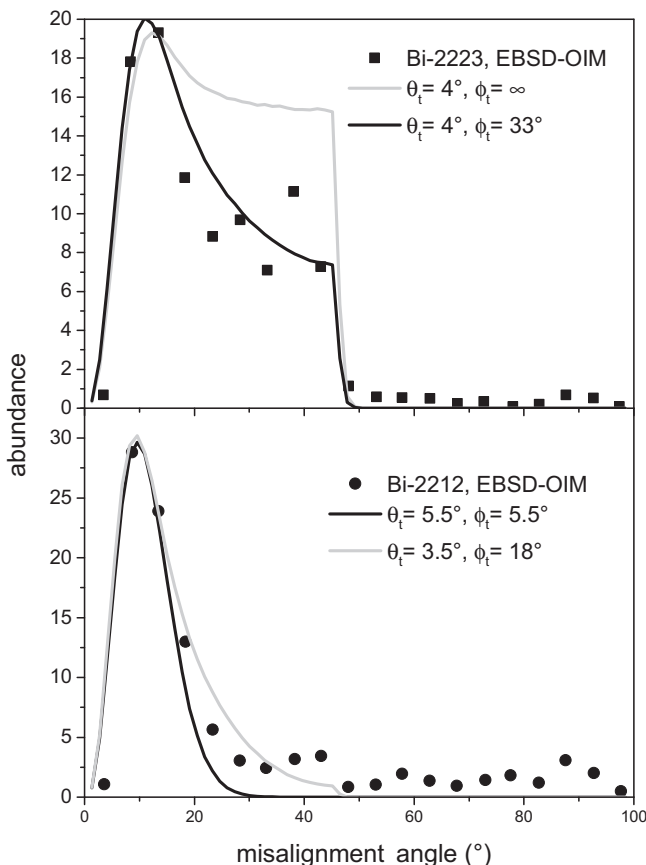
FIG. 6. Distribution density of grain boundary angles in Bi-2223 tapes (topes panel) and Bi-2212 wires (bottom panel). Experimental data (symbols) were extracted from Ref. [24].

pure out-of-plane texture. The experimental data do not show this plateaulike behavior, or the peak is much higher than the plateau; hence, the in-plane orientation is likely not totally random. This is taken into account by adding a weak in-plane alignment ($\phi_t = 33°$), which leads to a much better agreement with the experiment (black line). The bottom panel refers to a Bi-2212 wire, where a local biaxial texture enables a high critical current. The experimental data can be reasonably well described by a similar in- and out-of-plane texture of about 5.5° or assuming a high out-of-plane texture (3.5°) and a weaker in-plane alignment. The latter is supported by the step at 45° in the experimental data. However, the plateau between 30° and 45° cannot be described either way. This in turn leads to the conclusion that the Gaussian distribution of the grain boundary angle is a useful approximation for Bi-2212 and 2223 but does not rigorously apply.

The critical current densities predicted on the basis of these distribution densities are represented by the stars in the bottom panel of Fig. 5. A value of 4×10^5 A cm^{-2} is obtained with $\theta_t = 3.5°$ and $\phi_t = 18°$, and $\theta_t = 5.5°$ and $\phi_t = 5.5°$ result in 6.8×10^5 A cm^{-2}. The latter value is in excellent agreement with the experimental data since about 6×10^5 A cm^{-2} were reported for the Bi-2212 wire at 1 T, the lowest field available [24]. The model somewhat underestimates the current density in the Bi-2223 tape. It predicts 1.1×10^5 A cm^{-2} for $\theta_t = 4°$ and $\phi_t = 33°$, while the self-field J_c of the tape is certainly above 2×10^5 A cm^{-2} (experimental data are available only for fields down to 2 T).

Another study on grain alignment and the resulting J_c is available for K-doped Ba-122 [5]. The distribution density of the grain boundary angles given in Fig. 5 of that paper cannot be described well by the Gaussian distributions, Eqs. (10) and (11). Therefore, the data for the bar graph were extracted and linearly interpolated for the calculations, which predict a J_c of 4.4×10^5 A cm^{-2}. This value cannot be directly compared with experimental data since only high-field data are available at low temperature. The behavior of the volume pinning force $F_p = J_c B \propto b^{0.64}(1 - b)^{2.3}$ observed at high temperatures [5] was hence used to extrapolate the high-field data to the self-field, which was estimated self-consistently from $B^{self} \approx \mu_0 J_c d/2$ with the sample thickness d. $J_c \approx 4.8 \times 10^5$ A cm^{-2} is obtained, which agrees with the value predicted by the percolation model.

Untextured, polycrystalline materials cannot be modeled because the behavior of J_c across grain boundaries with misalignment angles above 45° is unknown. However, by looking at the data of Katase *et al.* [2] [see their Fig. 1(b)], it is tempting to speculate that $J_c^{GB}(\alpha)$ becomes constant above 30° in iron-based superconductors since the values at 30° and 45° are very similar. This flattening was also pointed out by Iida *et al.* [20]. With this assumption about high*angle grain boundaries our approach predicts a current density of 2.2×10^5 A cm^{-2}, while the highest reported self-fields J_c reach 2×10^5 A cm^{-2} [25,26].

A constant J_c^{GB} above 30° does not change the above calculations for textured conductors significantly because grain boundaries with angles above 30° do not significantly contribute to the current transport either in the theoretical analysis shown in Fig. 5 (maximum texture angle of 15°) or in the K-doped Ba-122 tape [5].

IV. DISCUSSION

The agreement between the model and the experimental data is astonishing, given the various assumptions and simplifications, in particular the reduction of the grain boundary properties to one parameter and a Gaussian distribution of the grain orientation. Note that there is no free parameter since all parameters (J_d, J_0, α_c, p_c) were fixed in accordance with literature values before the calculations. The behavior of the grain boundaries is based on experiments with pulsed laser deposition (PLD) films on bicrystalline substrates, which may or may not be representative of natural grain boundaries. Even in these films the scatter of data is considerable. Also no common agreement on the values of the depairing current density J_d of the various materials has been reached so far. Since the parameter selection was subjective (but not biased in view of the results), some coincidence is certainly responsible for the agreement, and a discussion of quantitative differences is pointless. There are good reasons for the approach to overestimate the critical currents in polycrystalline conductors: The superconducting matrix is assumed to be perfect (no voids, secondary phases, etc.), and the average self-field is certainly smaller at artificial grain boundaries than in the conductors under consideration. On the other hand, there are good reasons for the opposite as well: The critical current density along the very planar grain boundaries resulting from PLD is smaller than those across meandering grain boundaries [22], which often arise from other synthesis techniques. Percolating currents could preferentially cross grain boundaries under a reduced Lorentz force, and last but not least, the large aspect ratio of the grains, in particular in the BiSCCO compounds, could enable a much higher macroscopic (longitudinal) current density than the local (mainly transversal) intergrain current densities [27] (see the brick-wall model [6,7]).

The model is restricted so far to the self-field limit and to textured materials mainly because of the lack of the respective experimental data on grain boundary currents. The extension of the model to untextured materials or materials containing a significant fraction of grain boundaries with misalignment angles above 45° will be straightforward when the corresponding experimental data or theoretical predictions become available. Predicting in-field currents might be more complex because the orientation of the local field with respect to the grain boundary becomes important and is hard to address within this approach. However, a model successfully describing the field dependence of J_c in untextured Ba-122, where high-angle grain boundaries dominate the current flow, was proposed by Hecher *et al.* [28]. That model also neglects any details of the current flow. The empirical prefactor (it is also called J_0 in Ref. [28], but it is different from J_0 used in Eqs. (3) and (4)) could be calculated with the mean-field percolation approach when data for currents across high-angle grain boundaries become available.

V. CONCLUSIONS

A model for the quantitative prediction of the macroscopic critical currents based on experimental data for the texture and the grain boundary properties was developed and successfully applied to Bi-2212 tapes, Bi-2212 wires, and Ba-122 tapes.

The good agreement between prediction and experiment indicates that the simplified grain boundary physics covers the essential physics of imperfectly textured high-temperature superconductors. For (perfect) uniaxial texture (out-of-plane), the currents are suppressed to 9% and 1.5% compared to highly biaxially textured materials in the iron-based and cuprate superconductors, respectively. A reliable prediction for untextured materials is not possible because the relevant grain boundaries have misorientation angles above 45° in that case, and very few experimental data exist for such high-angle grain boundaries.

APPENDIX

1. Grain boundary angle between two adjacent grains

Without loss of generality, the crystallographic axes of the first grain are assumed to be parallel to the *x*, *y*, and *z* axes of the Cartesian coordinate system. The crystallographic axes of the other grain can be considered as the axes of another coordinate system, and the unit vectors of $\vec{a}$, $\vec{b}$, and $\vec{c}$ define the transformation matrix between these two coordinate systems:

$$T = \begin{pmatrix} - & \vec{e_a} & - \\ - & \vec{e_b} & - \\ - & \vec{e_c} & - \end{pmatrix}. \tag{A1}$$

T then also defines the rotation of the two crystallographic lattices, and the rotation angle can be easily obtained from

$$\mathrm{tr}(T) = 1 + 2\cos\alpha. \tag{A2}$$

The rotation axis is the eigenvector of T to the eigenvalue 1.

2. Distribution of grain boundary angles

We start with two perfectly aligned grains (i.e., $\alpha = 0$), their (normalized) crystallographic axes defining our coordinate system. In order to change the orientation of the second grain, we first establish its in-plane misorientation by a rotation about $\vec{e_z}$

$$R_{\mathrm{in}} = \begin{pmatrix} \cos\phi_{\mathrm{in}} & -\sin\phi_{\mathrm{in}} & 0 \\ \sin\phi_{\mathrm{in}} & \cos\phi_{\mathrm{in}} & 0 \\ 0 & 0 & 1 \end{pmatrix}. \tag{A3}$$

Next, the out-of-plane misorientation is defined by choosing a new orientation of $\vec{c}$ with its unit vector

$$\vec{e_c} = \begin{pmatrix} \sin\theta\cos\phi \\ \sin\theta\sin\phi \\ \cos\theta \end{pmatrix}; \tag{A4}$$

θ then defines the out-of-plane misorientation angle, and ϕ has to be determined such that the in-plane misorientation remains unaltered. This is achieved by a rotation of the second

grain about the axis orthogonal to the plane spanned by $\vec{e_c}$ and $\vec{e_z}$, i.e., $\vec{n} = \vec{e_z} \times \vec{e_c}/|\vec{e_z} \times \vec{e_c}| = (-\sin\phi, \cos\phi, 0)^T$. The resulting rotation matrix is given by

$$R_{\text{out}} = \begin{pmatrix} n_1^2(1-\cos\theta)+\cos\theta & n_1 n_2(1-\cos\theta)-n_3\sin\theta & n_1 n_3(1-\cos\theta)+n_2\sin\theta \\ n_1 n_2(1-\cos\theta)+n_3\sin\theta & n_2^2(1-\cos\theta)+\cos\theta & n_2 n_3(1-\cos\theta)-n_1\sin\theta \\ n_1 n_3(1-\cos\theta)-n_2\sin\theta & n_2 n_3(1-\cos\theta)+n_1\sin\theta & n_3^2(1-\cos\theta)+\cos\theta \end{pmatrix}. \qquad (A5)$$

The rotation (or misalignment) angle can be calculated from Eq. (A2) with $T = R_{\text{out}}R_{\text{in}}$:

$$\cos\alpha = \tfrac{1}{2}(\cos\theta + \cos\theta\cos\phi_{\text{in}} + \cos\phi_{\text{in}} - 1). \qquad (A6)$$

For a random orientation, ϕ_{in} is equally distributed on $[0\,2\pi]$ [i.e., $f_{\text{in}}(\phi_{\text{in}}) = 1/2\pi$], and θ is distributed as $f_{\text{out}}(\theta) = \tfrac{1}{2}\sin\theta$ on $[0\,\pi]$. The distribution function for α is obtained by calculating the fraction of grains with a misalignment angle less than or equal to α. ϕ_{in} can vary between zero and α, and $\cos\theta$ is, for a given α and ϕ_{in}, bounded by Eq. (A6). Equation (6) results from the corresponding integration:

$$F_\alpha(\alpha) = \int_0^\alpha \frac{1}{2\pi} d\phi_{\text{in}} \int_0^{\arccos\frac{2\cos\alpha-\cos\phi_{\text{in}}+1}{1+\cos\phi_{\text{in}}}} \frac{1}{2}\sin\theta d\theta$$
$$= \frac{1}{2\pi}(\alpha - \sin\alpha). \qquad (A7)$$

If θ and ϕ_{in} are restricted to $\pi/2$ and $\pi/4$, respectively, the maximum misalignment angle can be calculated from Eq. (A6) by inserting these maximum values for θ and ϕ_{in}: $\alpha_{\text{max}} = \arccos\tfrac{1}{2}(\frac{1}{\sqrt{2}} - 1) = 1.7178 = 98.42°$. Different angular regions have to be considered in this case since the limits of the integration over ϕ_{in} in Eq. (A7) change: The upper limit is fixed to $\pi/4$ for $\alpha > \pi/4$ (maximum in-plane misalignment); the lower limit becomes larger than zero for $\alpha > \pi/2$. The latter is necessary since a small ϕ_{in} cannot result in such high misalignment angles. The actual lower limit for a given $\alpha > \pi/2$ is calculated again from Eq. (A6).

With the correct limits, the distribution functions given in Eqs. (7)–(9) are obtained.

3. Numerical simulations

Since it turned out to be difficult to derive an analytical expression for nonrandom grain orientations, numerical simulations were performed. Cubic grains (typically about 150^3) were arranged on a simple cubic lattice (coordination number of 6). Their orientation was chosen as outlined above [in- and out-of-plane rotations, Eqs. (A3) and (A5)], but allowing a preferred grain orientation according to Eqs. (10) and (11), if desired. The coordinate system of the first grain is transformed into the system of the other grain by $T = T_2 T_1^T$, where T_1 and T_2 are the rotation matrices of the two grains defined as above ($T_i = R_{\text{out},i}R_{\text{in},i}$, $i = 1, 2$). The rotation angle is then, in principle, obtained from relation (A2). However, the symmetries have to be taken into account, which results in

$$\cos\alpha = \tfrac{1}{2}[\max(|T_{1,1}| + |T_{2,2}|, |T_{1,2}| + |T_{2,1}|) + |T_{3,3}| - 1] \qquad (A8)$$

($T_{i,j}$ refer to the matrix elements of T). The absolute values reflect inversion symmetry; the maximum refers to an exchange of the a and b axes.

Finally, the grain boundary angles of all pairs of grains were calculated and assigned to the respective angular interval to derive the distribution density.

[1] H. Hilgenkamp and J. Mannhart, Rev. Mod. Phys. **74**, 485 (2002).

[2] T. Katase, Y. Ishimaru, A. Tsukamoto, H. Hiramatsu, T. Kamiya, K. Tanabe, and H. Hosono, Nat. Commun. **2**, 409 (2011).

[3] D. C. Larbalestier, J. Jiang, U. P. Trociewitz, F. Kametani, C. Scheuerlein, M. Dalban-Canassy, M. Matras, P. Chen, N. C. Craig, P. J. Lee *et al.*, Nat. Mater. **13**, 375 (2014).

[4] I. Pallecchi, A. Leveratto, V. Braccini, V. Zunino, and A. Malagoli, Supercond. Sci. Technol. **30**, 095005 (2017).

[5] H. Huang, C. Yao, C. Dong, X. Zhang, D. Wang, Z. Cheng, J. Li, S. Awaji, H. Wen, and Y. Ma, Supercond. Sci. Technol. **31**, 015017 (2018).

[6] L. N. Bulaevskii, J. R. Clem, L. I. Glazman, and A. P. Malozemoff, Phys. Rev. B **45**, 2545 (1992).

[7] L. N. Bulaevskii, L. L. Daemen, M. P. Maley, and J. Y. Coulter, Phys. Rev. B **48**, 13798 (1993).

[8] B. Hensel, G. Grasso, and R. Flükiger, Phys. Rev. B **51**, 15456 (1995).

[9] G. N. Riley, A. P. Malozemoff, Q. Li, S. Fleshler, and T. G. Holesinger, JOM **49**, 24 (1997).

[10] D. C. van der Laan, J. Schwartz, B. ten Haken, M. Dhallé, and H. J. N. van Eck, Phys. Rev. B **77**, 104514 (2008).

[11] E. D. Specht, A. Goyal, and D. M. Kroeger, Phys. Rev. B **53**, 3585 (1996).

[12] R. Haslinger and R. Joynt, Phys. Rev. B **61**, 4206 (2000).

[13] E. E. Specht, A. Goyal, and D. M. Kroeger, Supercond. Sci. Technol. **13**, 592 (2000).

[14] Y. Nakamura, T. Izumi, and Y. Shiohara, Physica C (Amsterdam, Neth.) **371**, 275 (2002).

[15] B. B. Zeimetz, B. A. Glowacki, and J. E. Evetts, Eur. Phys. J. B **29**, 359 (2002).

[16] M. Eisterer, M. Zehetmayer, and H. W. Weber, Phys. Rev. Lett. **90**, 247002 (2003).

[17] M. Eisterer, W. Häßler, and P. Kováč, Phys. Rev. B **80**, 174516 (2009).

[18] S. C. van der Marck, Phys. Rev. E **55**, 1514 (1997).

[19] G. Deutscher, R. Zallen, and J. Adler, *Percolation Structures and Processes*, Ann. Israel Phys. Soc. Vol. 5 (Adam Hilger, Bristol, 1983).

[20] K. Iida, J. Hänisch, and C. Tarantini, Appl. Phys. Rev. **5**, 031304 (2018).

[21] R. Held, C. W. Schneider, J. Mannhart, L. F. Allard, K. L. More, and A. Goyal, Phys. Rev. B **79**, 014515 (2009).

[22] D. M. Feldmann, T. G. Holesinger, R. Feenstra, C. Cantoni, W. Zhang, M. Rupich, X. Li, J. H. Durrell, A. Gurevich, and D. C. Larbalestier, J. Appl. Phys. **102**, 083912 (2007).

[23] W. Häßler, P. Kovac, M. Eisterer, A. B. Abrahamsen, M. Herrmann, C. Rodig, K. Nenkov, B. Holzapfel, T. Melisek, M. Kulich *et al.*, Supercond. Sci. Technol. **23**, 065011 (2010).

[24] F. Kametani, J. Jiang, M. Matras, D. Abraimov, E. E. Hellstrom, and D. Larbalestier, Sci. Rep. **5**, 8285 (2015).

[25] S. Pyon, T. Suwa, T. Tamegai, K. Takano, H. Kajitani, N. Koizumi, S. Awaji, N. Zhou, and Z. Shi, Supercond. Sci. Technol. **31**, 055016 (2018).

[26] J. D. Weiss, C. Tarantini, J. Jiang, F. Kametani, A. A. Polyanskii, D. C. Larbalestier, and E. E. Hellstrom, Nat. Mater. **11**, 682 (2012).

[27] G. Hammerl, A. Herrnberger, A. Schmehl, A. Weber, K. Wiedenmann, C. W. Schneider, and J. Mannhart, Appl. Phys. Lett. **81**, 3209 (2002).

[28] J. Hecher, T. T Baumgartner, J. D. Weiss, C. Tarantini, A. Yamamoto, J. Jiang, E. E. Hellstrom, D. C. Larbalestier, and M. Eisterer, Supercond. Sci. Technol. **29**, 025004 (2016).